Chinese Chemical Letters 31 (2020) 535–538

Contents lists available at ScienceDirect

Chinese Chemical Letters

journal homepage: www.elsevier.com/locate/cclet

Communication

New ZnCe catalyst encapsulated in SBA-15 in the production of 1,3-butadiene from ethanol

Yujun Zhao[a,*], Sijia Li[a], Zheng Wang[a], Shengnian Wang[b,*], Shengping Wang[a], Xinbin Ma[a]

[a] Key Laboratory for Green Chemical Technology of Ministry of Education. Collaborative Innovation Center of Chemical Science and Engineering, School of Chemical Engineering and Technology, Tianjin University, Tianjin 300072, China
[b] Chemical Engineering, Institute for Micromanufacturing, Louisiana Tech University, Ruston, LA 71272, United States

ARTICLE INFO

Article history:
Received 14 March 2019
Received in revised form 11 April 2019
Accepted 16 April 2019
Available online 17 April 2019

Keywords:
1,3-Butadiene
Ethanol
SBA-15
Dehydrogenation
Aldol-condensation

ABSTRACT

ZnO-CeO_2/SBA-15 catalysts were prepared by two kinds of solid-state grinding method and used for the production of 1,3-butadiene (1,3-BD) from ethanol. A mixture of SBA-15 (with or without organic template) and metal precursors were ground in solid-state. The obtained catalysts were characterized by TG, N_2 adsorption-desorption, TEM, XRD, Py-FTIR and NH_3-TPD techniques. Superior dispersion of metal oxides and more exposed acid sites were achieved on the catalyst $10Zn_1Ce_5$-AS with the presence of organic template in SBA-15 during the solid-state grinding process. The catalytic performance was evaluated in a fixed-bed reactor and a 1,3-butadiene selectivity of as high as 45% is achieved. This is attributed to the coupling effect of Zn and Ce species in the mesopores of SBA-15, in which Zn promotes ethanol dehydrogenation and Ce enhances aldol-condensation, respectively. Additionally, solvent-free method inspires new catalyst synthesis strategy for the production of 1,3-butadiene from ethanol.

As an important organic feedstock, 1,3-butadiene is widely used in the production of polybutadiene, synthetic rubber, polymer resin, and many other petrochemical products [1,2]. In current world market, 1,3-butadiene is mainly produced by separating from the C4 fraction following ethylene manufacturing *via* the steam cracking of naphtha. However, its production is largely tied with the petroleum resources.

With the advancement of bioethanol technology and abundant ethanol source in recent years, synthesizing 1,3-butadiene from renewable ethanol draws great interests [3,4]. The synthesis of 1,3-butadiene from ethanol have two major routes: one-step direct synthesis of 1,3-butadiene and two-step production process (ethanol is first partially converted to acetaldehyde and acetaldehyde is further reacted with ethanol to obtain 1,3-butadiene) [1,5,6]. The two-step process has advantages of low reaction temperature and high selectivity to 1,3-butadiene, but the process is more complicated and the equipment investment is higher in comparison with one-step method. For one-step process, how to fabricate an efficient catalyst with high 1,3-butadiene selectivity is always a big challenge.

The reaction mechanism of this system is complicated and involves five consecutive reaction steps (Scheme 1) [7,8]: (i) Ethanol is dehydrogenated to acetaldehyde; (ii) Two acetaldehyde molecules are converted to acetaldol by aldol-condensation; (iii) Acetaldol is dehydrated to form crotonaldehyde; (iv) Meerwein–Ponndorf–Verley (MPV) reaction between crotonaldehyde and ethanol to obtain crotyl alcohol; (v) 1,3-Butadiene is generated by the dehydration of crotyl alcohol. In this multiple-step reaction system, ethanol dehydrogenation and aldol-condensation are two critical steps [9], which require two different active sites of the catalyst. For ethanol dehydrogenation, redox active sites are required, typically provided by copper oxide [1,5,8], silver [1,10] or zinc oxide [1,11]. The aldol-condensation reaction requires Lewis acid or base sites. The Lewis acid sites are generally supplied by elements from the IIIB, IVB and VB groups in the periodic table, such as Y [12], Zr [13], Hf [14] and Ta [15]. Magnesium oxide is the typical candidate for Lewis base sites [16]. An excellent ethanol-to-1,3-butadiene catalyst requires wise coupling of these two types of active sites. Baerdemaeker *et al.* developed a stable and active catalyst by combining Hf(IV) with Zn(II), in which the adding of Zn(II) to the Hf(IV)-containing catalyst was crucial important to force the Hf(IV) into catalyzing the acetaldehyde condensation rather than the ethanol dehydration [17]. Dai *et al.* prepared a bi-component Zn-Y catalyst confined in zeolite cages, and exhibited a high 1,3-butadiene selectivity of 63% in the one-step process [18].

Ordered mesoporous silica (OMS) materials, such as SBA-15 [19], KIT-6 [19], MCF [20] and MCM-41 [21], were explored as catalyst supports in this reaction system. Their large pore size and specific surface area were believed to improve the accessibility of

* Corresponding authors.
E-mail addresses: yujunzhao@tju.edu.cn (Y. Zhao), swang@latech.edu (S. Wang).

https://doi.org/10.1016/j.cclet.2019.04.038

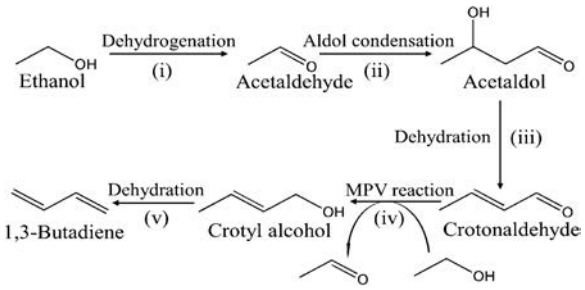

Scheme 1. Reaction mechanism of ethanol to 1,3-butadiene.

active sites for reactants and intermediates, effectively solving the mass transfer and coking formation during 1,3-butadiene production from ethanol [19]. Chae *et al.* have reported that Ta/OMS catalysts had better coke tolerance, catalytic longevity and catalytic activity than conventional silica-based catalysts [19]. For these catalysts, the metal was generally loaded by wet impregnation method, which was not time and energy effective. However, solvent-free method has not yet reported in the ethanol to 1,3-butadiene system.

In this study, we compared two kind of ZnO-CeO_2/SBA-15 catalysts with different solid-state grinding method (SBA-15 with or without organic template P123 (PEO-PPO-PEO) during grinding process). The limited space between the template P123 and the silica wall of SBA-15 prevents the infiltrated metal oxides from forming large aggregates, and achieving a high dispersion of oxides. The effect of the template P123 in SBA-15 on the formation process and physicochemical properties of the catalysts, as well as the catalytic performance in ethanol-to-1,3-butadiene were discussed in detail. In addition, as a solvent-free method, this solid-state grinding strategy is energy effectively and environmentally friendly in comparison with wet impregnation method.

The mesoporous silica SBA-15 support was prepared by a hydrothermal synthesis method reported by Zhao *et al.* [22]. The as-prepared SBA-15 material (with organic template) was recovered by filtration, washed and dried. Then through calcination, the template-free SBA-15 material was obtained. The catalysts $10Zn_1Ce_5$-AS/$10Zn_1Ce_5$-CS were prepared by solid-state grinding the as-prepared/template-free SBA-15 with the metal precursors. 10Zn-AS and 10Ce-AS were only loaded single metal oxide. The detailed information about synthesis method was given in Supporting information.

In order to explore the decomposition process of catalysts, the as-prepared SBA-15, $10Zn_1Ce_5$-AS and $10Zn_1Ce_5$-CS were characterized by TG technique. As shown in Fig. 1a, the decomposition of template (P123) of as-prepared SBA-15 takes place between 150 °C and 280 °C, corresponding to a sharp DTG peak at 180 °C in Fig. 1b. As the temperature further rises, the subsequent weight loss is attributed to the removal of residual carbonaceous species [23]. The decomposition of $10Zn_1Ce_5$-CS presents two DTG peaks at 80 °C and 200 °C, which is the result of the removal of water and the thermal decomposition of $Zn(NO_3)_2$ and $Ce(NO_3)_3$, respectively. For $10Zn_1Ce_5$-AS, the TG curve shows 50% weight loss due to the decomposition of organic template and metal salt precursors. However, the decomposition temperature of P123 is at around 235 °C, much higher than that for SBA-15 support itself (180 °C) [22]. Similar phenomenon has also been observed on CuO/SBA-15 [24] and ZnO/SBA-15 [25]. This is believed as the result of the strong interaction between metal ions and the head group of PEO molecules. The creation of helical crown ether-like metal-PEO complexes inevitably impedes the decomposition of the nonionic surfactant [26]. And the interaction contributes to a high dispersion of oxides on the mesoporous support.

Fig. S2 (Supporting information) shows the nitrogen adsorption-desorption isotherms and the pore size distribution for various samples. All samples display Langmuir Type IV isotherms with a H4 hysteresis loop (Fig. S2a), indicating the presence of mesoporous structure with uniform pore size [27]. Compared with the parent SBA-15 sample, the hysteresis of the modified samples shift to lower P/P_0 values, suggesting that a decrease of pore size after active species loading [28], which is also evidenced by their pore size distribution profiles shown in Fig. S2b. Therefore, it can be inferred that the zinc-cerium species are to some extent dispersed into the mesopores of the parent SBA-15. According to the physical properties of catalysts listed in Table S1 (Supporting information), the specific surface area and pore volume of $10Zn_1Ce_5$-CS are much smaller than $10Zn_1Ce_5$-AS, which can be explained by partial blockage of pores caused by aggregation of zinc and cerium species [29]. It also suggests that the presence of organic template can help well distribute the precursors of zinc and cerium in the mesopores of SBA-15 during the solid-state grinding process.

The surface morphology and pore structure of SBA-15 and two SBA-15 supported catalysts ($10Zn_1Ce_5$-AS and $10Zn_1Ce_5$-CS) were further revealed by TEM and X-ray diffraction results. As shown in Fig. S3a (Supporting information), SBA-15 exhibits the highly ordered pore-arrangement. Such regular pore patterns are well reserved in $10Zn_1Ce_5$-AS, as shown in Fig. S3b (Supporting information). Moreover, no nanoparticles can be observed in the TEM images, which elucidates a well dispersed state of the oxides in the mesopores of SBA-15. But for $10Zn_1Ce_5$-CS, some large particles are obviously seen on SBA-15 support, implying the agglomeration of ZnO or CeO_2 particles (Fig. S3c in Supporting information).

Low-angle X-ray diffraction measurement was also performed to reveal the possible structural changes of SBA-15 support induced by oxides loading. As shown in Fig. 2a, the characteristic peaks of SBA-15 are clearly observed on samples of SBA-15 support alone and $10Zn_1Ce_5$-AS. This further endorses the TEM results that the ordered mesoporous structure of SBA-15 largely retains when the template is not removed during the solid-state grinding

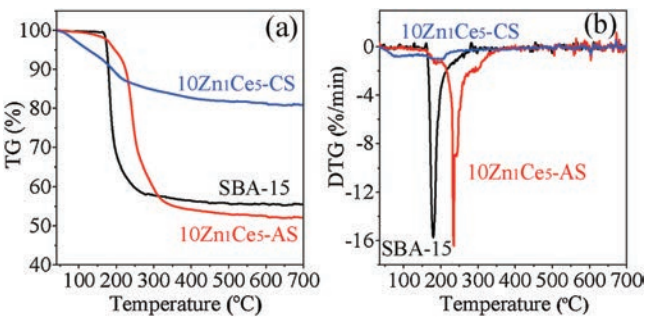

Fig. 1. (a) TG curves and (b) DTG curves of the uncalcined SBA-15, $10Zn_1Ce_5$-AS and $10Zn_1Ce_5$-CS.

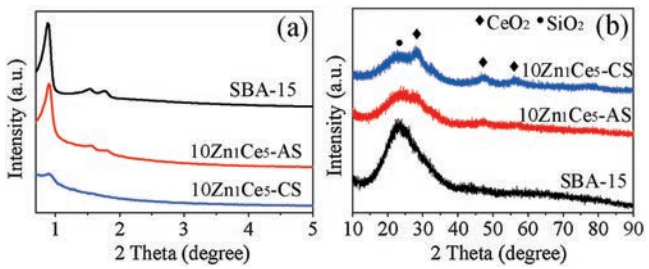

Fig. 2. (a) Low-angle and (b) wide-angle XRD patterns of SBA-15, $10Zn_1Ce_5$-AS and $10Zn_1Ce_5$-CS.

process for catalyst preparation. However, for $10Zn_1Ce_5$-CS catalyst, the characteristic peaks of SBA-15 support in the low-angle XRD spectrum (Fig. 2a) become much weaker, implying the destruction of the ordered mesoporous structure. The aggregation of metal oxide species inside or outside of the mesopores could be the reason for this change, which can be further evidenced by the wide-angle X-ray diffraction measurement.

As shown in Fig. 2b, the peaks of CeO_2 at 28.6°, 47.5° and 56.3° appear in the XRD pattern of $10Zn_1Ce_5$-AS and $10Zn_1Ce_5$-CS samples beside a broad peak at 23° which is assigned to amorphous silica. This suggests that aggregation of cerium species is inevitable during the solid-state grinding process. Furthermore, these peaks are much stronger from $10Zn_1Ce_5$-CS than that from $10Zn_1Ce_5$-AS, implying more serious aggregation of cerium species at the absence of organic template in the SBA-15 support. In either case (with or without organic template), no characteristic peaks of ZnO are found, indicating the better dispersion of ZnO in both samples. The TEM and X-ray diffraction results are in good agreement and suggest that the importance of the organic template on the dispersion of metal oxides during the solid-grinding process. It can be inferred that the limited space between the organic template and the silica wall of SBA-15 makes it difficult for oxide particles to aggregate, which helps improve the dispersion of oxides on SBA-15 [30].

The acidic properties of catalysts were measured by Py-FTIR and NH_3-TPD. Py-FTIR was performed to analyze the type of acid sites. As can be seen from Fig. 3a, both $10Zn_1Ce_5$-AS and $10Zn_1Ce_5$-CS have only Lewis acid sites (around 1450 cm^{-1}), and no Bronsted acid sites (around 1540 cm^{-1}) are found. The FTIR peak intensity also suggests more Lewis acid sites on $10Zn_1Ce_5$-AS than that on $10Zn_1Ce_5$-CS. The strength and amount of acid sites were further characterized by NH_3-TPD. As shown in Fig. 3b, the parent SBA-15 has almost no acidity. However, after being modified by ZnO and CeO_2, it appears two desorption peaks at about 180 °C and 290 °C, indicating the existence of two types of acid sites. The desorption peak around 180 °C is attributed to the weak acid sites of the samples and the strong acid sites are located near 290 °C. Moreover, the total amounts of acid sites on $10Zn_1Ce_5$-AS are much more than $10Zn_1Ce_5$-CS, which is in consistent with the Py-FTIR results. When taking consideration of the better dispersion of CeO_2 on $10Zn_1Ce_5$-AS than $10Zn_1Ce_5$-CS, we can conclude that the well dispersed cerium species could be the reason for the increased acid sites.

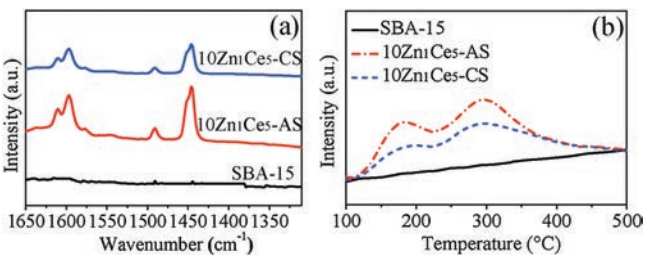

Fig. 3. (a) Py-FTIR spectra and (b) NH_3-TPD profiles for SBA-15, $10Zn_1Ce_5$-AS and $10Zn_1Ce_5$-CS.

The catalytic activity of catalysts was examined in the synthesis of 1,3-butadiene from ethanol at the same reaction conditions (375 °C, 1.62 h^{-1}). As shown in Table 1, remarkably higher ethanol conversion and 1,3-butadiene selectivity are achieved on $10Zn_1Ce_5$-AS than $10Zn_1Ce_5$-CS. As confirmed by the characterization results, the existence of template P123 in the parent SBA-5 can help embed the precursors of ceria and zinc into the mesopores during the grinding process, leading to a higher dispersion of metal oxides in the final catalyst. On the one hand is the strong interaction between metal ions and template, the other is the confined space between the organic template and the silica wall of SBA-15. The enhanced dispersion of the ceria species can provide more Lewis acid sites, which is believed to be the key reason for the higher activity and selectivity of catalyst. Similar observations were also found in some other pioneer work of various catalysts. Ivanova *et al.* reported that the activity of catalysts correlated well with the amount of Lewis acid sites of Zr-containing molecular sieves [21]. Pomalaza *et al.* have also observed a strong correlation between the selectivity of 1,3-butadiene and the amount of acid sites on various Zn(II)-Ta(V) based-catalyst [31]. For $10Zn_1Ce_5$-CS catalyst, the absence of template resulted in the agglomeration of CeO_2 particles, leading to less exposure of Lewis acid sites. Therefore, the catalyst presents a lower activity in the conversion of ethanol to 1,3-butadiene. In addition, the catalysts supporting only one metal oxide were also evaluated. For 10Zn-AS, the main product is acetaldehyde, which may be attributed to the redox site of zinc that promotes only the dehydrogenation of ethanol. Due to the absence of enough acid sites, the aldol-condensation is inhibited, resulting in a much low selectivity of 1,3-butadiene. As regard to 10Ce-AS, ethanol is effectively dehydrated to produce ethylene, suggesting that the acid sites of cerium mainly catalyze the dehydration of ethanol. About bi-component Zn-Ce catalyst, the addition of zinc to Ce-containing catalyst inhibits the dehydration of ethanol effectively and enhances the dehydrogenation of ethanol, and the aldol-condensation ability of cerium is promoted as well. This result was in consistent with Zn-Hf catalyst reported by Baerdemaeker *et al.* [17]. The synergy between the dehydrogenation sites and Lewis acid sites determines the product distribution in the reaction. A matched combination of the two kinds of active sites could improve the formation of 1,3-butadiene with a higher yield.

A slow declining trend on the conversion of ethanol is shown in Fig. 4, which indicates the slow deactivation of $10Zn_1Ce_5$-AS. The selectivity of 1,3-butadiene is sustained in 20 h, while acetaldehyde is increased and ethylene production is slowly decreased as the reaction continues. It suggests that the deactivation of acid sites which are responsible for aldol-condensation could be the main reason for the coke formation and catalyst deactivation. But overall, our $10Zn_1Ce_5$-AS exhibits pretty good stability despite the slow deactivation of the catalyst.

In this study, we report a highly efficient ZnO-CeO_2/SBA-15 catalyst prepared by modified solid-state grinding method. Despite good dispersion of ZnO, the presence of organic template in the as-prepared SBA-15 improves the dispersion of CeO_2. This is contributed to the limited space between the template and the

Table 1
Catalytic performance of catalysts at 375 °C and WHSV of 1.62 h^{-1} for 5 h.

Sample	Conversion (%)	Selectivity (%)						1,3-BD yield (%)
		Ethylene	Propylene	Acetaldehyde	Butene	1,3-BD	Ethyl ether	
$10Zn_1Ce_5$-AS	78.7	22.1	3.9	21.6	5.6	45.3	1.6	35.7
$10Zn_1Ce_5$-CS	34.9	39.0	1.3	41.0	1.6	15.0	2.2	5.2
10Zn-AS	66.3	22.1	1.9	56.0	0.7	17.9	1.4	11.9
10Ce-AS	17.6	82.6	0.7	4.5	0.8	4.8	6.5	1.4

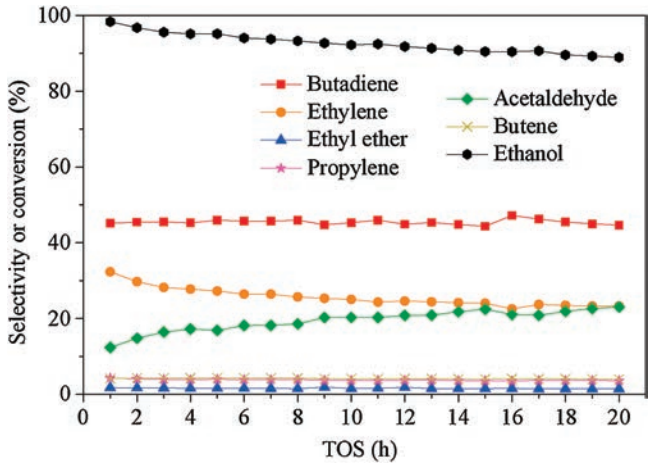

Fig. 4. The stability of $10Zn_1Ce_5$-AS in 20 h (reaction conditions: T = 375 °C, WHSV = 1.08 h^{-1}).

silica wall of SBA-15, and to the strong interaction between metal ions and template. The enhanced dispersion of the ceria species provides more Lewis acid sites, therefore a higher butadiene selectivity of about 45% is achieved on $10Zn_1Ce_5$-AS, in which the coupling effect of ethanol dehydrogenation and aldol-condensation is realized effectively. As a solvent-free method, this strategy could provide an inspiration on the catalyst preparation for the synthesis of 1,3-butadiene from ethanol.

Acknowledgement

We are grateful to the financial support from the National Natural Science Foundation of China (No. 21878227).

Appendix A. Supplementary data

Supplementary material related to this article can be found, in the online version, at doi:https://doi.org/10.1016/j.cclet.2019.04.038.

References

[1] E.V. Makshina, W. Janssens, B.F. Sels, P.A. Jacobs, Catal. Today 198 (2012) 338–344.
[2] H.X. Zhang, Y. Li, C.Q. Zhang, et al., Chin. Chem. Lett. 21 (2010) 361–364.
[3] A. Walter, F. Rosillo-Calle, P. Dolzan, E. Piacente, K. Borges da Cunha, Biomass Bioenerg. 32 (2008) 730–748.
[4] J.M. Otero, G. Panagiotou, L. Olsson, Adv. Biochem. Eng. Biotechnol. 108 (2007) 1–40.
[5] W.J. Toussaint, J.T. Dunn, D.R. Jachson, Ind. Eng. Chem. Res. 39 (1947) 120–125.
[6] G. Pomalaza, M. Capron, V. Ordomsky, F. Dumeignil, Catalysts 6 (2016) 203.
[7] H.E. Jones, E.E. Stahly, B.B. Corson, J. Am. Chem. Soc. 71 (1949) 1822–1828.
[8] C. Angelici, M.E. Velthoen, B.M. Weckhuysen, P.C. Bruijnincx, ChemSusChem 7 (2014) 2505–2515.
[9] V.L. Sushkevich, I.I. Ivanova, V.V. Ordomsky, E. Taarning, ChemSusChem 7 (2014) 2527–2536.
[10] W. Janssens, E.V. Makshina, P. Vanelderen, et al., ChemSusChem 8 (2015) 994–1008.
[11] O.V. Larina, P.I. Kyriienko, S.O. Soloviev, Catal. Lett. 145 (2015) 1162–1168.
[12] T. Yan, W. Dai, G. Wu, et al., ACS Catal. 8 (2018) 2760–2773.
[13] V.L. Sushkevich, D. Palagin, I.I. Ivanova, ACS Catal. 5 (2015) 4833–4836.
[14] G.M. Cabello González, R. Murciano, A.L. Villanueva Perales, et al., Appl. Catal. A-Gen. 570 (2019) 96–106.
[15] P. Müller, S.P. Burt, A.M. Love, et al., ACS Catal. 6 (2016) 6823–6832.
[16] Q. Zhu, B. Wang, T. Tan, ACS Sustain. Chem. Eng. 5 (2016) 722–733.
[17] T. De Baerdemaeker, M. Feyen, U. Müller, et al., ACS Catal. 5 (2015) 3393–3397.
[18] W. Dai, S. Zhang, Z. Yu, et al., ACS Catal. 7 (2017) 3703–3706.
[19] T.W. Kim, J.W. Kim, S.Y. Kim, et al., Chem. Eng. J. 278 (2015) 217–223.
[20] J.L. Cheong, Y. Shao, S.J.R. Tan, et al., ACS Sustain. Chem. Eng. 4 (2016) 4887–4894.
[21] V.L. Sushkevich, I.I. Ivanova, E. Taarning, Green Chem. 17 (2015) 2552–2559.
[22] D. Zhao, J. Feng, Q. Huo, et al., Science. 279 (1998) 548–552.
[23] F. Kleitz, W. Schmidt, F. Schüth, Microporous Mesoporous Mater. 65 (2003) 1–29.
[24] Y. Xu, Q. Jiang, Y. Cao, et al., Adv. Funct. Mater. 14 (2004) 1113–1123.
[25] Q. Jiang, Z.Y. Wu, Y.M. Wang, et al., J. Mater. Chem. A. 16 (2006) 1536–1542.
[26] S.A. Bagshaw, J. Mater. Chem. A. 11 (2001) 831–840.
[27] R. Schmidt, E.W. Hansen, M. Stacker, D. Akporiaye, O.H. Ellestad, J. Am. Chem. Soc. 117 (1995) 4049–4056.
[28] A. Yin, X. Guo, W.L. Dai, K. Fan, J. Phys. Chem. C 113 (2009) 11003–11013.
[29] Y. Wang, J. Liao, J. Zhang, et al., AICHE J. 63 (2017) 2839–2849.
[30] Y.M. Wang, Z.Y. Wu, L.Y. Shi, J.H. Zhu, Adv. Mater. 17 (2005) 323–327.
[31] G. Pomalaza, G. Vofo, M. Capron, F. Dumeignil, Green Chem. 20 (2018) 3203–3209.